

Quantum Hall Effect without Chern Bands

Benjamin Michen^{1,*} and Jan Carl Budich^{1,2,†}

¹*Institute of Theoretical Physics, Technische Universität Dresden and Würzburg-Dresden Cluster of Excellence ct.qmat, 01062 Dresden, Germany*

²*Max Planck Institute for the Physics of Complex Systems, Nöthnitzer Str. 38, 01187 Dresden, Germany*
(Dated: June 10, 2025)

The quantum Hall effect was originally observed in a two-dimensional electron gas forming Landau levels when exposed to a strong perpendicular magnetic field, and has later been generalized to Chern insulators without net magnetization. Here, further extending the realm of the quantum Hall effect, we report on the robust occurrence of an integer quantized transverse conductance at the onset of disorder in a microscopic lattice model all bands of which are topologically trivial (zero Chern number). We attribute this remarkable phenomenon to the energetic separation of substantial but non-quantized Berry fluxes within the topologically trivial bands. Adding a random disorder potential then nudges the system into a stable quantum Hall phase from an extended critical regime of the clean system obtained by placing the Fermi energy within a broad window in either of the trivial bands. Our results are corroborated by extensive numerical transport simulations as well as the analysis of several complementary topological markers.

The quantum Hall effect, one of the most remarkable phenomena occurring in nature, is of foundational importance to the broad research field of topological matter [1–10]. Establishing topology as the rationale behind physical robustness, the experimental observation of a transverse conductance σ_{xy} quantized in units of e^2/h has been explained with theory in terms of a topological invariant known as the first Chern number [11–14]. This represents a pioneering example of the by now well established paradigm of topological Bloch bands characterized by global properties, the discrete value of which remains unchanged under continuous perturbations [15–18]. Adiabatic continuity is in this context largely synonymous with the existence of a finite energy gap that must close at a topological quantum phase transition for a topological property to change [19, 20].

Surprisingly, in this work we provide strong evidence that the topological quantization of the Hall conductance can occur in an extended parameter regime of a microscopic lattice model, both Bloch bands of which are topologically trivial. Specifically, when placing the Fermi energy E_F within a wide energy window in either band of our model, switching on a simple on-site disorder potential with amplitude W stabilizes a Quantum Hall effect with $\sigma_{xy} = e^2/h$, while σ_{xy} has a non-universal E_F -dependent value at $W = 0$ (see Fig. 1). We attribute this behavior to the formation of a topologically non-trivial mobility gap with the onset of disorder [21–25]. In this light, the clean metallic situation with E_F inside the eligible window may be seen as an extended critical region that is nudged into a stable quantum Hall phase by a generic disorder potential.

On the other hand, we emphasize that the underlying clean band structure of our model may be continuously deformed into a trivial atomic insulator. That way, all

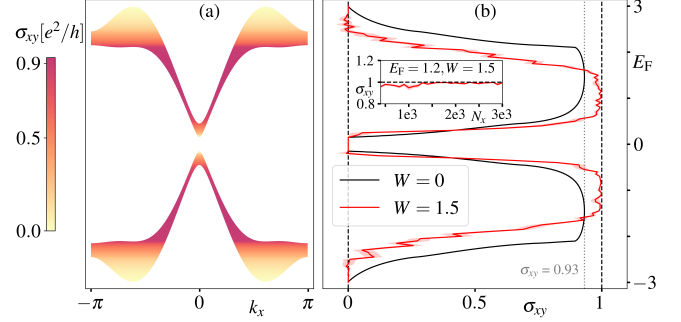


FIG. 1. (a) Band structure of the free Hamiltonian \hat{H}_0 [see Eq. (1)]. Colorcode indicates Hall conductance $\sigma_{xy}^{W=0}(E_F)$ of the clean system as a function of Fermi energy E_F , which is proportional to the Berry curvature accumulated up to E_F [cf. Eq. (2)]. (b) $\sigma_{xy}^W(E_F)$ at $W = 0$ in black and at disorder strength $W = 1.5$ in red for system size $N_x = 2000$, $N_y = 500$, averaged over $S = 40$ disorder realizations, where the shaded corridor indicates the standard error of the sample. Inset: Finite size scaling at $E_F = 1.2$ as a function of N_x at fixed aspect ratio $N_x/N_y = 4$. Other model parameters in all plots are $r = 1.5$, $\epsilon_1 = 0.3$, $\epsilon_2 = 2$, $\gamma = 2$, and $\gamma_2 = 0.3$.

structure is removed from the entire microscopic lattice system without a topological quantum phase transition, which clearly makes the phenomena reported in this work quite different from the familiar quantum Hall scenarios based on Chern bands and Landau levels, respectively. As we detail below, our findings also differ qualitatively from several other settings in which topological phenomena have been identified in unconventional relation to Chern numbers [26–32].

Besides performing extensive numerical simulations on the transport properties of our model system (see Figs. 1–3) based on the software package Kwant [33–35], we verify that a topological invariant defined in the mobility gap [36–38] characterized by a finite localization length of bulk states indeed confirms our predictions regarding

* benjamin.michen@tu-dresden.de

† jan.budich@tu-dresden.de

the quantization of Hall conductance. A careful analysis of the spectral localizer gap structure [39–44] in the considered system provides further complementary evidence corroborating our results (see Fig. 4).

Minimal two-banded lattice model. — We introduce a minimal lattice model specified by the Hamiltonian

$$\hat{H} = \hat{H}_0 + \hat{W}, \quad (1)$$

where \hat{H}_0 is a free translation-invariant two-band Hamiltonian and $\hat{W} = W \sum_{j_x, j_y} \sum_{\alpha=a,b} f_{j, \alpha} c_{j, \alpha}^\dagger c_{j, \alpha}$ is the disorder potential with overall strength $W \geq 0$ and random amplitudes $f_{j, \alpha}$ drawn independently from the uniform distribution on the interval $[-1, 1]$. In reciprocal space, the translation-invariant part is fully specified by the Bloch Hamiltonian $h_0(\mathbf{k}) = \mathbf{d}(\mathbf{k}) \cdot \boldsymbol{\sigma}$, with $\boldsymbol{\sigma}$ the vector of standard Pauli matrices and the coefficient vector $d_x(\mathbf{k}) = \gamma \sin(k_x)$, $d_y(\mathbf{k}) = \lambda(k_x) \sin(k_y)$, $d_z(\mathbf{k}) = \gamma_2[r - \cos(2k_x)] - \lambda(k_x) \cos(k_y)$, and $\lambda(k_x) = \epsilon_1 + \epsilon_2(1 - \cos(k_x))/2$, which corresponds to a tight-binding model on a two-dimensional (2D) square lattice with unit lattice constant. Containing only nearest-neighbor, plaquette diagonal, and next-nearest-neighbor in x -direction hopping terms, our model is local and fully microscopic [45]. In the following, we will discuss its design principles and exemplify our findings using the parameters $r = 1.5$, $\epsilon_1 = 0.3$, $\epsilon_2 = 2$, $\gamma = 2$, and $\gamma_2 = 0.3$, for which both bands are topologically trivial (zero Chern number), and there is a finite band gap [see Fig. 1(a)].

Berry flux and transport without disorder. — To make a finite transverse conductance plausible, the topologically trivial Bloch bands of our model accommodate local (in reciprocal space) Berry fluxes that, however, compensate each other within each band when integrated over the first Brillouin zone, and are non-quantized. To get a feeling for the transport properties of the clean system ($W = 0$), we find it helpful to express the zero temperature Hall conductance as a function of Fermi energy in terms of the accumulated Berry flux up to the Fermi energy, i.e.

$$\sigma_{xy}^{W=0}(E_F) = \frac{e^2}{h} \frac{1}{2\pi} \int_{E_{\mathbf{k}} < E_F} d^2k \mathcal{F}, \quad (2)$$

where \mathcal{F} is the Berry curvature [45]. The colorcode in Fig. 1(a) and the $W = 0$ plot line in Fig. 1(b) visualizes the landscape of $\sigma_{xy}^{W=0}(E_F)$.

We would like to emphasize two points in this light. First, the zero value of $\sigma_{xy}^{W=0}(E_F)$ in the band gap hallmarks the topologically trivial nature of the bands. Second, the approximate plateau of $\sigma_{xy}^{W=0}(E_F)$ within either band has a non-quantized (and non-universal with model parameters) value, and merely reflects a certain energetic separation of the aforementioned local Berry fluxes within the bands. Since there is no spectral gap or mobility gap in the energy windows of finite Hall conductance in the clean case, it is not surprising that the value of $\sigma_{xy}^{W=0}$ is not quantized and can be tuned with

the hopping parameters of our model. Clearly, for E_F inside the bands, the metallic nature of the clean model is reflected in an extensive value of $\sigma_{xx}^{W=0}$.

Transport properties at finite disorder. — Now, consider switching on disorder, i.e. $W > 0$. In 2D, the theory of Anderson localization then tells us that even a small random potential should localize (almost) all states and introduce a mobility gap, which in turn should force the Hall conductance to a quantized value. At small W , it seems natural that σ_{xy} may jump to the closest possible integer value, which is then retained on further increasing the disorder strength. This intuition agrees with field-theoretical studies of disordered models with non-trivial Chern bands [6–9, 46, 47], which study plateau broadening in weakly disordered Chern insulators where the phase transition between different integer quantum Hall (IQH) plateaus concurs with half-integer values of the accumulated Berry flux [cf. Eq. (2)]. Our present work extends the scope of this phenomenology to systems without Chern bands. Importantly, once protected by a finite mobility gap, a quantized value of σ_{xy} is topologically protected against any small perturbation, just as for the conventional Quantum Hall scenario starting from an underlying Chern band structure and Landau level structure, respectively. Remarkably, extensive numerical analysis of our model system fully supports this rationale of a robust quantum Hall effect without Chern bands, as we present in detail in the following [see $W = 1.5$ line and inset in Fig. 1(b) for a first impression].

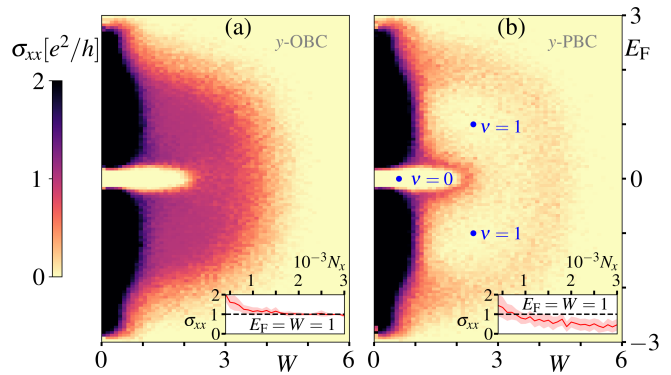


FIG. 2. (a) Two-terminal conductance for a system with $N_x = 600$, $N_y = 150$ sites and OBC in y -direction. Transport occurs in x -direction. (b) Two-terminal conductance as in (a) but for PBC in y -direction. Winding number ν [see Eq. (4)] indicated at the blue points in parameter space. Insets: Size scaling of σ_{xx} for $E_F = 1$ and $W = 1$ over N_x at constant aspect ratio $N_x/N_y = 4$ with standard deviation indicated as a shaded corridor. All results are averaged over $S = 20$ disorder realizations and model parameters are $r = 1.5$, $\epsilon_1 = 0.3$, $\epsilon_2 = 2$, $\gamma = 2$, $\gamma_2 = 0.3$.

Using the software package KWANT [33–35], we start our series of numerical simulations with a basic two-terminal linear response calculation of the longitudinal conductance σ_{xx} as a function of Fermi Energy E_F and disorder strength W for a mesoscopic system of

$N_x = 600$, $N_y = 150$. We note that the aspect ratio of $N_x/N_y = 4$ in this and the following simulations is chosen due to the anisotropic nature of our model system. The leads are modeled with a width of 50 sites attached to the center of each vertical face, i.e. at $x = 1$ and $x = N_x$ around $y = N_y/2$. The dispersion of the leads is set to $t_L[\cos(k_x) + \cos(k_y)]\sigma_0$ with $t_L = 10$. In Fig. 2, we compare the resulting transport properties for OBC and PBC so as to highlight the effect of edge state transport. For OBC [see Fig. 2(a)], we indeed find an extended region where the conductance is quantized to one, indicating a topologically protected edge state. By contrast, for PBC [see Fig. 2(b)], any edge states disappear and the sample is found to be insulating precisely in the parameter regime, where conductance quantization is most precise for OBC. We also note a strong $\sigma_{xx} > \frac{e^2}{h}$ at weak disorder strength $W < 1$ for any E_F inside the bands. We attribute this to an expected finite size effect: when the average localization length becomes comparable to system size, an extensive number of evanescent bulk modes contributes to the longitudinal conductance. The inset of Fig. 2(a) quantifies the dependence of the evanescent conductance on N_x . All data in Fig. 2 is the average of $S = 20$ independent disorder realizations.

We note that Fig. 2(b) also provides a complementary view on the non-quantized conductance of the clean system that is nudged into an IQH phase through the disorder potential, relating to previous work on systems with topological bands [10, 31, 32]. There, the finite Berry fluxes of opposite sign separate and flow towards mutual annihilation. Importantly, Berry charges do not annihilate within the same band but recombine inter-band, thus forming an inner arc and an outer arc in the $E_F - W$ parameter plane. The phase of quantized Hall conductance is enclosed by these two arcs.

We now directly probe the transverse (or Hall) conductance σ_{xy} at finite $W = 1.5$. This amounts to modeling our transport simulation as a standard four-terminal setting for measuring the Hall conductance [48, 49]. The system size is set to $N_x = 2000$, $N_y = 500$ and the leads are attached to the center of all four sample faces, with a lead width of 50 sites at the vertical faces and 100 sites at the horizontal faces due to larger localization lengths in this direction. In Fig. 1(b), the resulting numerical data showing the quantization of σ_{xy} to $\frac{e^2}{h}$ in an extended window of E_F as the average over $S = 40$ independent disorder realizations is presented. As expected for a finite system with limited self-averaging properties, averaging over a sample of disorder realizations improves the precision of the quantization. However, we emphasize that also the single measurements clearly fluctuate around the quantized value as opposed to the non-universal value of the clean system [45]. The inset of Fig. 1(b) shows how deviations from the quantized value decay with increasing system size for a fixed value of E_F within the plateau region. We note that the energy window of the quantized Hall plateau at $W = 1.5$ differs from the window of large non-quantized Berry flux at $W = 0$ in agreement

with the continuous deformation of the region of quantized transport in Fig. 2 as a function of W . However, we emphasize that there is no bulk band gap closing between $W = 0$ and $W = 1.5$.

Complementary to the above four-terminal setup, we now explore a larger parameter range in the $W - E_F$ plane by computing σ_{xy} through the Kubo-Bastin formula [50–52] for linear response conductivity

$$\sigma_{xy}(E_F, T) = \frac{ie^2\hbar}{V} \int_{-\infty}^{\infty} dE f(E_F - E, T) \times \text{Tr} \left[v_x \frac{dG^+}{dE} v_y \rho(E) - v_x \rho(E) v_y \frac{dG^-}{dE} \right]. \quad (3)$$

Here, $f(E - E_F, T)$ is the Fermi distribution at temperature T , $v_\alpha = -(i/\hbar)[R_\alpha, H]$ denotes the velocity operator as induced by the position operator R_α , $\rho(E) = \delta(E - H)$ is the density of states (DOS), and $G^\pm = [E \pm i0^+ - H]^{-1}$ the retarded and advanced Green's function (GF), respectively. In the interest of numerical efficiency, the DOS and GF may be systematically approximated by an expansion in Chebyshev polynomials to order M , with the expansion coefficients determined from a Monte-Carlo evaluation of the trace using R random phase vectors [53–55]. Together with the number of disorder iterations S , these parameters control the numerical accuracy in evaluating Eq. (3), see [45] for technical details.

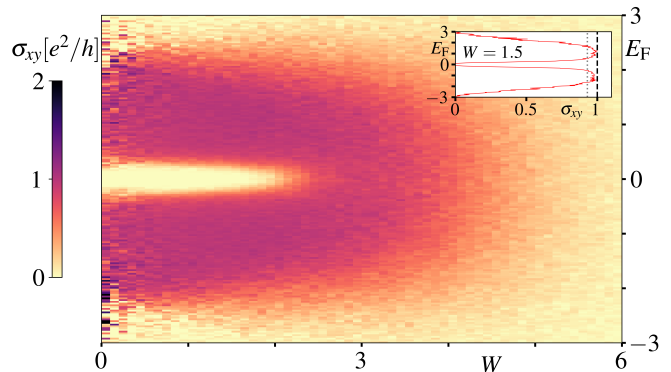


FIG. 3. Hall conductance as a function of W and E_F for a system of $N_x = 600$, $N_y = 150$ sites with PBC, obtained from the Chebyshev expansion of the Kubo-Bastin formula (3) with $M = 1500$, $R = 5$, and $S = 10$. Model parameters are $r = 1.5$, $\epsilon_1 = 0.3$, $\epsilon_2 = 2$, $\gamma = 2$, $\gamma_2 = 0.3$. Inset: Calculation with increased accuracy using $M = 2500$ and $S = 50$ for $W = 1.5$. The maximal clean Hall conductance $\sigma_{xy} = 0.93$ is shown as a dotted gray line for reference [cf. Fig. 1(b)].

Fig. 3 shows σ_{xy} as a function of W and E_F at $T = 0$. These results fully confirm the edge state picture discussed above in the context of the longitudinal conductance [cf. Fig. 2(a)]. We attribute minor deviations of σ_{xy} from its quantized value in the core IQH parameter regime to the combination of finite-size effects and the approximate nature of the numerical evaluation. For

a quantitative analysis of finite-size effects, we refer the reader to the inset of Fig. 1(b).

Topology of conductance quantization. — When the Fermi energy lies inside a mobility gap at finite W , for which zero longitudinal transmission amplitude is a sufficient condition here, a topological invariant may be defined directly for the reflection part R of the unitary S -matrix. Specifically, upon introducing twisted boundary conditions perpendicular to the direction of transport by means of a flux angle ϕ , the integer quantized winding number

$$\nu = \frac{1}{2\pi} \oint_0^{2\pi} d\phi \left(\frac{\partial}{\partial \phi} \arg[\det[R(\phi, E)]] \right) \quad (4)$$

of the reflection matrix counts the charge pumped between the cylinder edges for a full twist of the boundary phase, which then corresponds to σ_{xy} for PBC in units of $\frac{e^2}{h}$ [36–38]. We calculate this invariant at multiple points in the phase diagram and indicate the result in Fig. 2(b), which further corroborates the topological nature of the IQH phase reported in this work.

As a complementary diagnostic tool for topology, we now analyze the spectral localizer, which is defined as the following Hermitian matrix

$$L(x, y, E) = \sigma_z \otimes (H - E) + \kappa \sigma_x \otimes (R_x - x) + \kappa \sigma_y \otimes (R_y - y) \quad (5)$$

for a system in two spatial dimensions and symmetry class A [18, 56]. Here, R_α denotes the position operator for the respective coordinate, x, y are real numbers representing a position in real space, and the parameter κ plays the role of balancing the weight of H and the position operators [39–43]. A crucial prerequisite of topological robustness is then provided by the bulk localizer gap

$$g_L(E) = \min_{x, y \in \text{bulk}} |\text{spec}[L(x, y, E)]|, \quad (6)$$

where $\text{spec}[\dots]$ denotes the set of all eigenvalues. For an energy E located in a spectral gap of H , a finite localizer gap $g_L(E)$ can be proven to exist for suitably chosen κ . In the presence of a bulk localizer gap, the index

$$Q(x, y, E) = \frac{1}{2} \text{sig}[L(x, y, E)], \quad (7)$$

where the signature $\text{sig}[L(x, y, E)]$ denotes the difference in the number of positive and negative eigenvalues, is well-defined and a constant integer for $x, y \in \text{bulk}$. Physically, Q measures the number of chiral edge states encircling the system at energy E [39–43]. We emphasize that the assumption of a spectral gap does not apply to our present analysis at $W = 0$. However, it has been observed that $g_L(E)$ can remain finite even if there is no spectral or mobility gap at E , which is still a subject of active research both from a physical and a mathematical perspective [32, 42].

In our model system, for a choice of $\kappa \approx 0.4$, we indeed find that a localizer gap opens deep inside the bulk band, which is accompanied by a non-trivial index $Q = -1$ (see Fig. 4). Contributing to the ongoing discussion about the role of $g_L(E)$ in metallic situations, we argue that the data in Fig. 4 still predicts the formation of a stable IQH phase in the presence of a generic random potential. In particular, at small disorder strength, for which all eigenvalues of \tilde{W} are smaller than $g_L(E)$, the localizer gap cannot close by virtue of Weyl’s inequality [32, 43, 45]. However, in the thermodynamic limit infinitesimal strength of disorder should suffice to cause a mobility gap due to Anderson localization, for which the localizer index does predict a chiral edge state surrounding the system [44], which by means of the bulk boundary correspondence is tantamount to an IQH phase.

Comparing the accumulated Berry flux with the localizer gap (see Fig. 4), we note that $\sigma_{xy}^{W=0}(E_F) < 0.5 e^2/h$ corresponds well to regions of a topologically trivial ($Q = 0$) localizer gap. However, a finite topological localizer gap ($Q = -1$) is only clearly visible in part of the energetic region with $\sigma_{xy}^{W=0}(E_F) > 0.5 e^2/h$. While this may to some extent relate to subtle finite size effects (see [45] for details), we do not exclude that Q contains additional structure beyond rounding $\sigma_{xy}^{W=0}$ to integer values. We emphasize that none of these scenarios contradicts our findings regarding σ_{xy} at finite W .

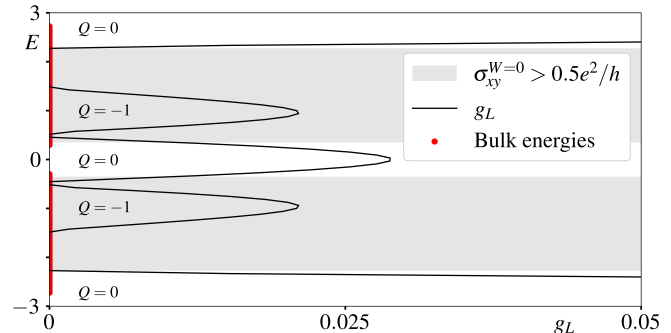


FIG. 4. Localizer gap g_L [cf. Eq. (6)] as a function of E for system size $N_x = 20$, $N_y = 20$ with scaling parameter $\kappa = 0.4$. The shown g_L is taken as the minimum of 100 reference positions inside the central Wigner-Seitz cell. Where g_L is finite, we indicate the associated value of the topological index Q [cf. Eq. (7)]. For reference, the clean bulk spectrum is shown in red and the energy window where $\sigma_{xy}^{W=0}(E_F) > 0.5 e^2/h$ [cf. Eq. (2)] is marked as a gray corridor. Model parameters are $r = 1.5$, $\epsilon_1 = 0.3$, $\epsilon_2 = 2$, $\gamma = 2$, $\gamma_2 = 0.3$.

Concluding Discussion. — We have demonstrated how a topologically stable quantum Hall effect may appear at the onset of disorder without any nontrivial Chern bands in the underlying band structure. To conclude, we would like to integrate our findings into a broader context by discussing their relation to previous work on non-standard (from a perspective of topological Bloch bands) topological phenomena.

In periodically driven (Floquet) systems far from equi-

librium, a counterpart of the IQH effect relating to Floquet chiral edge states has been reported despite zero Chern number of all bulk bands [29, 30]. However, there the underlying band structure is still topological and the chiral edge states can only be removed by changing a bulk topological invariant unique to Floquet systems, which makes the role of zero Chern numbers very different from our present work.

Moreover, in a topological band structure with a trivial band that is energetically sandwiched in between two Chern bands and connected to them via topologically protected chiral edge states, a topological fine structure has recently been reported [32]. There, a bulk localizer gap inside the trivial band is connected to a disorder-driven transition where the two Chern bands do not directly recombine but both recombine with (substructure of) the trivial band. However, this leaves open the main question addressed in our present work, namely whether a quantum Hall effect can occur in a system without any topological bands and protected chiral edge states in the underlying band structure, respectively.

Finally, a phase known as the topological Anderson insulator (TAI) has been reported [26–28]. There, starting from a trivial gapped band structure, disorder drives a topological quantum phase transition (associated with a bulk gap closing in the effective band structure) into a Chern insulator phase. While generic disorder as a physical mechanism for turning a trivial insulator into a topological one is both powerful and intriguing, from a

more general perspective this scenario is quite similar to entering a conventional Chern insulator phase by tuning a band structure parameter. By contrast, in our present setting, no topological quantum phase transition in the form of a bulk gap closing of the underlying band structure is responsible for the formation of the IQH phase. Instead, it occurs with the onset of disorder while a bulk gap closing only occurs a quite large disorder strength $W > 2$ (cf. Fig. 2).

With the advent of Chern insulators generalizing from the specific setting of Landau levels, it was demonstrated that a magnetic field or net magnetization is not necessary for the occurrence of the quantum Hall effect [57]. In this general context, our present work further relaxes the conditions for the generic occurrence of the quantum Hall effect by exemplifying how the energetic separation of substantial but non-quantized Berry fluxes in topologically trivial band structures can be sufficient. Our findings thus further widen the habitat of topologically quantized physical observables.

Acknowledgments. — We would like to thank Emil J. Bergholtz, Ion Cosma Fulga, and Björn Trauzettel for discussions. We acknowledge financial support from the German Research Foundation (DFG) through the Collaborative Research Centre SFB 1143 (Project-ID 247310070), the Cluster of Excellence ct.qmat (Project-ID 390858490). Our numerical calculations were performed on resources at the TU Dresden Center for Information Services and High Performance Computing (ZIH).

-
- [1] K. v. Klitzing, G. Dorda, M. Pepper, *New Method for High-Accuracy Determination of the Fine-Structure Constant Based on Quantized Hall Resistance*, *Phys. Rev. Lett.* **45**, 494 (1980).
- [2] R. E. Prange, *Quantized Hall resistance and the measurement of the fine-structure constant*, *Phys. Rev. B* **23**, 4802(R) (1981).
- [3] R. B. Laughlin, *Quantized Hall conductivity in two dimensions*, *Phys. Rev. B* **23**, 5632(R) (1981).
- [4] D. J. Thouless, *Localisation and the two-dimensional Hall effect*, *J. Phys. C: Solid State Phys.* **14**, 3475 (1981).
- [5] B. I. Halperin, *Quantized Hall conductance, current-carrying edge states, and the existence of extended states in a two-dimensional disordered potential*, *Phys. Rev. B* **25**, 2185 (1982).
- [6] H. Levine, S. B. Libby, and A. M. Pruisken, *Electron Delocalization by a Magnetic Field in Two Dimensions*, *Phys. Rev. Lett.* **51**, 1915 (1983).
- [7] A.M.M. Pruisken, *On localization in the theory of the quantized hall effect: A two-dimensional realization of the Θ -vacuum*, *Nuclear Physics B* **235**, 277 (1984).
- [8] H. Levine, S. B. Libby, and A. M. Pruisken, *Theory of the quantized Hall effect (i)*, *Nuclear Physics B* **240**, 30 (1984).
- [9] D. E. Khmelnitskii, *Quantization of Hall conductivity*, *ZhETF Pisma Redaktsiiu* **38**, p. 454-458 (1983).
- [10] R. B. Laughlin, *Levitiation of Extended-State Bands in a Strong Magnetic Field*, *Phys. Rev. Lett.* **52**, 2304 (1984).
- [11] S. S. Chern, *Characteristic Classes of Hermitian Manifolds*, *Annals of Mathematics*, **47**, 1 (1946).
- [12] D. J. Thouless, M. Kohmoto, M. P. Nightingale, and M. den Nijs, *Quantized Hall Conductance in a Two-Dimensional Periodic Potential*, *Phys. Rev. Lett.* **49**, 405 (1982).
- [13] Q. Niu, D. J. Thouless, and Y.-S. Wu, *Quantized Hall conductance as a topological invariant*, *Phys. Rev. B* **31**, 3372 (1985).
- [14] M. Kohmoto, *Topological invariant and the quantization of the Hall conductance*, *Annals of Physics* **160**, 2 (1985).
- [15] M. Z. Hasan and C. L. Kane, *Colloquium: Topological insulators*, *Rev. Mod. Phys.* **82**, 3045 (2010).
- [16] X.-L. Qi and S.-C. Zhang, *Topological insulators and superconductors*, *Rev. Mod. Phys.* **83**, 1057 (2011).
- [17] C.-K. Chiu, J. C. Y. Teo, A. P. Schnyder, and S. Ryu, *Classification of topological quantum matter with symmetries*, *Rev. Mod. Phys.* **88**, 035005 (2016).
- [18] J. C. Budich and B. Trauzettel, *From the adiabatic theorem of quantum mechanics to topological states of matter*, *Rap. Res. Lett.* **7** (1-2), 109-129 (2013).
- [19] X. Chen, Z.-C. Gu, and X.-G. Wen, *Local unitary transformation, long-range quantum entanglement, wave function renormalization, and topological order*, *Phys. Rev. B* **82**, 155138 (2010).
- [20] X.-G. Wen, *Colloquium: Zoo of quantum-topological*

- phases of matter, *Rev. Mod. Phys.* **89**, 041004 (2017).
- [21] P. W. Anderson, *Absence of Diffusion in Certain Random Lattices*, *Phys. Rev.* **109**, 1492 (1958).
- [22] E. Abrahams, P. W. Anderson, D. C. Licciardello, and T. V. Ramakrishnan, *Scaling Theory of Localization: Absence of Quantum Diffusion in Two Dimensions*, *Phys. Rev. Lett.* **42**, 673 (1979).
- [23] F. Wegner, *The mobility edge problem: Continuous symmetry and a conjecture*, *Z Physik B.* **35**, 207–210 (1979).
- [24] P. A. Lee and D. S. Fisher, *Anderson Localization in Two Dimensions*, *Phys. Rev. Lett.* **47**, 882 (1981).
- [25] Ferdinand Evers and Alexander D. Mirlin, *Anderson transitions*, *Rev. Mod. Phys.* **80**, 1355 (2008).
- [26] J. Li, R.-L. Chu, J. K. Jain, and S.-Q. Shen, *Topological Anderson Insulator*, *Phys. Rev. Lett.* **102**, 136806 (2009).
- [27] C. W. Groth, M. Wimmer, A. R. Akhmerov, J. Tworzydło^{1,2}, and C. W. J. Beenakker, *Theory of the Topological Anderson Insulator*, *Phys. Rev. Lett.* **103**, 196805 (2009).
- [28] Y.-Y. Zhang, R.-L. Chu, F.-C. Zhang, and S.-Q. Shen, *Localization and mobility gap in the topological Anderson insulator*, *Phys. Rev. B* **85**, 035107 (2012).
- [29] M. S. Rudner, N. H. Lindner, E. Berg, and M. Levin, *Anomalous Edge States and the Bulk-Edge Correspondence for Periodically Driven Two-Dimensional Systems*, *Phys. Rev. X* **3**, 031005 (2013).
- [30] P. Titum, E. Berg, M. S. Rudner, G. Refaelli, and N. H. Lindner, *Anomalous Floquet-Anderson Insulator as a Nonadiabatic Quantized Charge Pump*, *Phys. Rev. X* **6**, 021013 (2016).
- [31] H. Liu, C. Fulga, J. K. Asboth, *Anomalous levitation and annihilation in Floquet topological insulators*, *Phys. Rev. Research* **2**, 022048(R) (2020).
- [32] H. Liu, C. Fulga, E. J. Bergholtz, J. K. Asboth, *Topological fine structure of an energy band*, [arXiv:2312.08436](https://arxiv.org/abs/2312.08436) (2023).
- [33] C. W. Groth, M. Wimmer, A. R. Akhmerov, X. Waintal, *Kwant: a software package for quantum transport*, *New J. Phys.* **16**, 063065 (2014).
- [34] P. R. Amestoy, I. S. Duff, J. S. Koster, J. Y. L'Excellent, *Accelerating Optimization of Parametric Linear Systems by Model Order Reduction*, *SIAM. J. Matrix Anal. & Appl.* **23** (1), 15 (2014).
- [35] To implement the Kubo-Bastin formula with PBC, we use the KWANT extension **KPM Tools**, which is largely based on ideas from: D. Varjas, M. Fruchart, A. R. Akhmerov, P. M. Perez-Piskunow, *Computation of topological phase diagram of disordered $\text{Pb}_{1-x}\text{Sn}_x\text{Te}$ using the kernel polynomial method*, *Phys. Rev. Research* **2**, 013229 (2020).
- [36] P. W. Brouwer, *Scattering approach to parametric pumping*, *Phys. Rev. B* **58**, R10135(R) (1998).
- [37] G. Bräunlich, G. M. Graf, and G. Ortelli, *Equivalence of Topological and Scattering Approaches to Quantum Pumping*, *Commun. Math. Phys.* **295**, 243–259 (2010).
- [38] I. C. Fulga, F. Hassler, and A. R. Akhmerov, *Scattering theory of topological insulators and superconductors*, *Phys. Rev. B* **85**, 165409 (2012).
- [39] T. A. Loring, *K-theory and pseudospectra for topological insulators*, *Annals of Physics* **356**, 383–416 (2015)
- [40] T. Loring and H. Schulz-Baldes, *Finite volume calculation of K-theory invariants*, [arXiv:1701.07455](https://arxiv.org/abs/1701.07455) (2017).
- [41] T. Loring and H. Schulz-Baldes, *The spectral localizer for even index pairings*, [arXiv:1802.04517](https://arxiv.org/abs/1802.04517) (2018).
- [42] A. Cerjan and T. A. Loring, *Local invariants identify topology in metals and gapless systems*, *Phys. Rev. B* **106**, 064109 (2022)
- [43] A. Cerjan and T. A. Loring, *Tutorial: Classifying Photonic Topology Using the Spectral Localizer and Numerical K-Theory*, *APL Photonics* **9**, 111102 (2024)
- [44] T. Stoiber, *A spectral localizer approach to strong topological invariants in the mobility gap regime*, [arXiv:2410.22214](https://arxiv.org/abs/2410.22214) (2024).
- [45] For more details on the model and the applied methods as well as additional data and extended derivations, please see online supplemental material.
- [46] P. M. Ostrovsky, I. V. Gornyi¹, and A. D. Mirlin, *Quantum Criticality and Minimal Conductivity in Graphene with Long-Range Disorder*, *Phys. Rev. Lett.* **98**, 256801 (2007).
- [47] M. Moreno-Gonzalez, J. Dieplinger, and A. Altland, *Topological quantum criticality of the disordered Chern insulator*, *Annals of Physics* **456**, 169258 (2023).
- [48] S. Datta, *Electronic Transport in Mesoscopic Systems*, Cambridge (1995).
- [49] G. Salerno, H. M. Price, M. Lebrat, S. Häusler, T. Esslinger, L. Corman, J.-P. Brantut, and N. Goldman, *Quantized Hall Conductance of a Single Atomic Wire: A Proposal Based on Synthetic Dimensions*, *Phys. Rev. X* **9**, 041001 (2019).
- [50] R. Kubo, *Statistical-Mechanical Theory of Irreversible Processes. I. General Theory and Simple Applications to Magnetic and Conduction Problems*, *Journal of the Physical Society of Japan* **12**, pp. 570-586 (1957).
- [51] A. Bastin, C. Lewinler, O. Betbeder-Matibet, and P. Nozieres, *Quantum oscillations of the hall effect of a fermion gas with random impurity scattering*, *J. Phys. Chem. Solids* **32**, 1811 (1971).
- [52] A. Crépieux and P. Bruno, *Theory of the anomalous Hall effect from the Kubo formula and the Dirac equation*, *Phys. Rev. B* **64**, 014416 (2001).
- [53] J. H. Garcia, L. Covaci, T. G. Rappoport, *Real-space calculation of the conductivity tensor for disordered topological matter*, *Phys. Rev. Lett.* **114**, 116602 (2015).
- [54] D. Ködderitzsch, K. Chadova, and H. Ebert, *Linear response Kubo-Bastin formalism with application to the anomalous and spin Hall effects: A first-principles approach*, *Phys. Rev. B* **92**, 184415 (2015).
- [55] A. Weisse, G. Wellein, A. Alvermann, H. Fehske, *The Kernel Polynomial Method*, *Rev. Mod. Phys.* **78**, 275 (2006).
- [56] A. Altland and M. R. Zirnbauer, *Nonstandard symmetry classes in mesoscopic normal-superconducting hybrid structures*, *Phys. Rev. B* **55**, 1142 (1997)
- [57] F. D. M. Haldane, *Model for a Quantum Hall Effect without Landau Levels: Condensed-Matter Realization of the "Parity Anomaly"*, *Phys. Rev. Lett.* **61**, 2015 (1988).

Appendix A: Details on the model

The translation-invariant part of the model from the main text is given by

$$\hat{H}_0 = \sum_{\mathbf{k}} \mathbf{c}_{\mathbf{k}}^\dagger h_0(\mathbf{k}) \mathbf{c}_{\mathbf{k}} \quad (\text{A1})$$

with fermionic creation operators $\mathbf{c}_{\mathbf{k}}^\dagger = (c_{\mathbf{k},a}^\dagger, c_{\mathbf{k},b}^\dagger)$ in reciprocal space and the Bloch Hamiltonian

$$h_0(\mathbf{k}) = \begin{pmatrix} d_z(\mathbf{k}) & d_x(\mathbf{k}) - id_y(\mathbf{k}) \\ d_x(\mathbf{k}) + id_y(\mathbf{k}) & -d_z(\mathbf{k}) \end{pmatrix}, \quad (\text{A2})$$

where

$$\begin{aligned} d_x(\mathbf{k}) &= \gamma \sin(k_x), \\ d_y(\mathbf{k}) &= \lambda(k_x) \sin(k_y), \\ d_z(\mathbf{k}) &= \gamma_2 [r - \cos(2k_x)] - \lambda(k_x) \cos(k_y), \end{aligned} \quad (\text{A3})$$

and $\lambda(k_x) = \epsilon_1 + \epsilon_2 [1 - \cos(k_x)]/2$. Using $\cos(x) \cos(y) = [\cos(x+y) + \cos(x-y)]/2$ and $\cos(x) \sin(y) = [\sin(x+y) - \sin(x-y)]/2$, we may rewrite this as

$$\begin{aligned} d_x(\mathbf{k}) &= \gamma \sin(k_x), \\ d_y(\mathbf{k}) &= (\epsilon_1 + \epsilon_2/2) \sin(k_y) - \epsilon_2 [\sin(k_x + k_y) - \sin(k_x - k_y)]/4, \\ d_z(\mathbf{k}) &= \gamma_2 [r - \cos(2k_x)] - (\epsilon_1 + \epsilon_2/2) \cos(k_y) + \epsilon_2 [\cos(k_x + k_y) + \cos(k_x - k_y)]/4. \end{aligned} \quad (\text{A4})$$

1. Real space Hamiltonian

The formulation in real space following from the Fourier transform $c_{\mathbf{k},\alpha}^\dagger = \frac{1}{\sqrt{N_x N_y}} \sum_{\mathbf{j}} e^{i\mathbf{k}\cdot\mathbf{j}} c_{\mathbf{j},\alpha}^\dagger$ and the relation

$$\sum_{\mathbf{j}} c_{\mathbf{j},\gamma}^\dagger c_{\mathbf{j}+\delta,\gamma'} = \sum_{\mathbf{k}} e^{i\mathbf{k}\delta} c_{\mathbf{k},\gamma}^\dagger c_{\mathbf{k},\gamma'}, \quad (\text{A5})$$

as

$$\begin{aligned} \hat{H}_0 &= \sum_{\mathbf{j}} \left[\gamma_2 r c_{\mathbf{j}}^\dagger \sigma^z c_{\mathbf{j}} + \left\{ \frac{\gamma}{2i} c_{\mathbf{j}}^\dagger \sigma^x c_{\mathbf{j}+\delta_x} + \frac{\epsilon_1 + \epsilon_2/2}{2i} c_{\mathbf{j}}^\dagger \sigma^y c_{\mathbf{j}+\delta_y} - \frac{\epsilon_2}{8i} c_{\mathbf{j}}^\dagger \sigma^y c_{\mathbf{j}+\delta_x+\delta_y} + \frac{\epsilon_2}{8i} c_{\mathbf{j}}^\dagger \sigma^y c_{\mathbf{j}+\delta_x-\delta_y} \right. \right. \\ &\quad \left. \left. - \frac{\epsilon_1 + \epsilon_2/2}{2} c_{\mathbf{j}}^\dagger \sigma^z c_{\mathbf{j}+\delta_y} + \frac{\epsilon_2}{8} c_{\mathbf{j}}^\dagger \sigma^z c_{\mathbf{j}+\delta_x+\delta_y} + \frac{\epsilon_2}{8} c_{\mathbf{j}}^\dagger \sigma^z c_{\mathbf{j}+\delta_x-\delta_y} - \frac{\gamma_2}{2} c_{\mathbf{j}}^\dagger \sigma^z c_{\mathbf{j}+2\delta_x} + \text{H.c.} \right\} \right]. \end{aligned} \quad (\text{A6})$$

2. Berry curvature and energies

The energies of the upper and lower band, which we denote here by \pm , are given by

$$E_{\pm} = \pm |\mathbf{d}| = \sqrt{[\gamma \sin(k_x)]^2 + [\lambda(k_x) \sin(k_y)]^2 + [\gamma_2 [r - \cos(2k_x)] - \lambda(k_x) \cos(k_y)]^2}. \quad (\text{A7})$$

The Berry curvature for each band can be expressed as

$$\mathcal{F}_{\pm}(\mathbf{k}) = \mp \hat{\mathbf{d}} \cdot [\partial_{k_x} \hat{\mathbf{d}} \times \partial_{k_y} \hat{\mathbf{d}}]/2 = \frac{\mp 1}{|\mathbf{d}|^3} \mathbf{d} \cdot [\partial_{k_x} \mathbf{d} \times \partial_{k_y} \mathbf{d}]/2, \quad (\text{A8})$$

where $\hat{\mathbf{d}} = \mathbf{d}/|\mathbf{d}|$ denotes the unit vector along \mathbf{d} . With

$$\partial_{k_x} \mathbf{d} = \begin{pmatrix} \gamma \cos(k_x) \\ [\epsilon_2/2] \sin(k_x) \sin(k_y) \\ 2\gamma_2 \sin(2k_x) - [\epsilon_2/2] \sin(k_x) \cos(k_y) \end{pmatrix}, \quad \partial_{k_y} \mathbf{d} = \begin{pmatrix} 0 \\ \lambda(k_x) \cos(k_y) \\ \lambda(k_x) \sin(k_y) \end{pmatrix}, \quad (\text{A9})$$

we find

$$\partial_{k_x} \hat{\mathbf{d}} \times \partial_{k_y} \hat{\mathbf{d}} = \begin{pmatrix} [\epsilon_2/2]\lambda(k_x) \sin(k_x) [\sin^2(k_y) + \cos^2(k_y)] - 2\gamma_2 \lambda(k_x) \sin(2k_x) \cos(k_y) \\ -\gamma \lambda(k_x) \cos(k_x) \sin(k_y) \\ \gamma \lambda(k_x) \cos(k_x) \cos(k_y) \end{pmatrix} \quad (\text{A10})$$

and ultimately

$$\begin{aligned} \mathbf{d} \cdot [\partial_{k_x} \mathbf{d} \times \partial_{k_y} \mathbf{d}] &= \lambda(k_x) \{ [\epsilon_2 \gamma / 2] \sin^2(k_x) - 2\gamma \gamma_2 \sin(k_x) \sin(2k_x) \cos(k_y) \\ &\quad - \gamma \lambda(k_x) \cos(k_x) \sin^2(k_y) \\ &\quad + \gamma \gamma_2 [r - \cos(2k_x)] \cos(k_x) \cos(k_y) - \gamma \lambda(k_x) \cos(k_x) \cos^2(k_y) \} \\ &= \lambda(k_x) \{ [\epsilon_2 \gamma / 2] \sin^2(k_x) - 2\gamma \gamma_2 \sin(k_x) \sin(2k_x) \cos(k_y) \\ &\quad + \gamma \gamma_2 [r - \cos(2k_x)] \cos(k_x) \cos(k_y) - \gamma \lambda(k_x) \cos(k_x) \}. \end{aligned} \quad (\text{A11})$$

With this, we have an analytic expression for Eq. (A8), which we can be evaluated on a discrete lattice in the First Brillouin zone together with the energy Eq. (A7). To obtain the $\sigma_{xy}^{W=0}(E_F)$ curve in the first figure of the main text in a computationally efficient manner, the resulting array can simply be sorted by energy and then summed up.

3. Non-topological edge states in Cylinder geometry

We find that the separation of topological charges within the bands can cause a pair of edge states to emerge at a boundary. However, this also depends on the direction of the boundary. Importantly, if an edge state emerges, it will always have an anti-chiral partner due to the vanishing total Chern number of the bands, i.e. it is not topologically protected and can be gapped out continuously.

To illustrate this, we compute the spectrum with PBC in x -direction and OBC in y -direction in Fig. 5(a). The edge states are highlighted by colors. The condition to be considered an edge state at the left / right edge is that 90% of the wave function amplitude is concentrated within the left / right 25% of the system. By contrast, in the spectrum with PBC in y -direction and OBC in x -direction presented in Fig. 5(b), no such states are present.

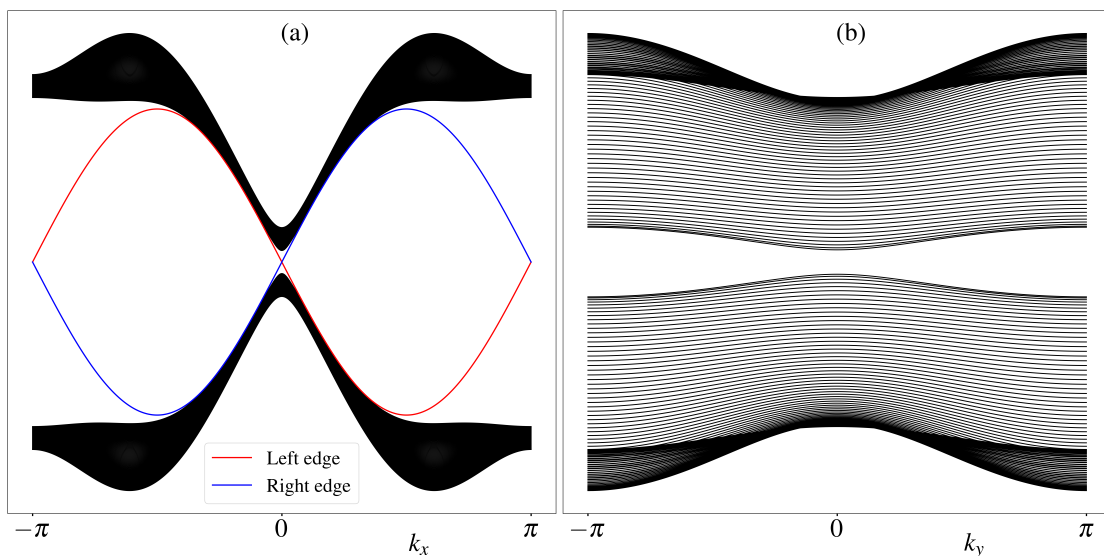


FIG. 5. Spectra for cylinders with a height of 100 unit cells for parameters $r = 1.5$, $\epsilon_1 = 0.3$, $\epsilon_2 = 2$, $\gamma = 2$, and $\gamma_2 = 0.3$ as a function of momentum in the circumferential direction. Edge states indicated if present. a) Result for OBC in y -direction, a pair of edge states emerges. b) Result for OBC in x -direction, no edge states present.

Appendix B: Additional data on the four terminal Hall conductance

To obtain the curve for the Hall conductance σ_{xy} presented in Fig. 1 of the main text, we model the system as a four terminal scattering experiment with KWANT [S9, S10]. Following Refs. [S1, S2], we extract the elements of the conductance tensor from the scattering amplitudes as

$$\sigma_{xx} = \frac{e^2}{h} T_{R \leftarrow L}, \quad \sigma_{xy} = \frac{e^2}{h} (T_{L \leftarrow T} - T_{L \leftarrow B}), \quad \sigma_{yx} = \frac{e^2}{h} (T_{B \leftarrow R} - T_{B \leftarrow L}), \quad \sigma_{yy} = \frac{e^2}{h} T_{T \leftarrow B}. \quad (\text{B1})$$

Here, $T_{p \leftarrow q}$ with $p, q = L$ (left), R (right), B (bottom), T (top) denotes the transmission amplitude from terminal β to α . In Fig. 6, we present the result for all elements of the conductance tensor. The quantized plateaus of the off-diagonal elements are accompanied by a vanishing of σ_{xx} and σ_{yy} . The peaks of the diagonal entries in the transition region between the Hall plateaus are indicative of a quantum phase transition. We illustrate the standard deviation of as a corridor (in Fig. 1 of the main text, we use the standard error which is smaller by a factor of $1/\sqrt{S}$ for visual clarity).

We also present a complementary way of extracting the Hall conductance from the four terminal scattering data. If all the transmission amplitudes $T_{p \leftarrow q}$ are known, the conductance matrix can be obtained as

$$G_{p,q} = -\frac{e^2}{h} T_{p \leftarrow q} + \delta_{p,q} \frac{e^2}{h} \sum_{q'} T_{q' \leftarrow p}. \quad (\text{B2})$$

The units and sign conventions are chosen such that the current at terminal p is obtained as $I_p = \sum_q G_{p,q} V_q$, where $V_q = -e\mu_q$ is the Voltage at terminal q , obtained from the chemical potential μ_q and the elementary charge $e = 1.602176634\text{E-}19\text{C}$.

As a complementary approach, given the conductance matrix it is possible to impose a current in one direction and determine the transverse voltage by solving the linear equation $\mathbf{I} = \mathbf{G}\mathbf{V}$. For σ_{xy} , this amounts to setting $I_L = I_x$, $I_R = -I_x$, $I_B = 0$, $I_T = 0$ with some arbitrary value I_x . This leaves the equation $\mathbf{I} = \mathbf{G}\mathbf{V}$ underdetermined, since the current does not change under a constant shift of all voltages. We can thus set, e.g., $V_T = 0$, which amounts to truncating the conductance matrix to the top left 3×3 block and solving for V_L , V_R , and V_B . The Hall voltage is then $V_{\text{Hall}} = V_B - V_T = V_B$ and the Hall conductance is found to be $\sigma_{xy} = I_x/V_{\text{Hall}} = I_x/V_B$. To determine σ_{yx} , the same the same procedure is used for the currents $I_L = 0$, $I_R = 0$, $I_B = I_y$, $I_T = -I_y$. This approach only yields a definite result for E_F inside the conductance plateaus, where the bulk of the system is insulating. There, however, it resolves the Hall plateaus very sharply and with small variance as we show in Fig. 7.

Appendix C: Kernel Polynomial Approach to the Kubo Bastin formula

In the interest of a self-contained presentation, we briefly review the kernel polynomial method (KPM) approach to computing the Kubo-Bastin formula that is implemented in the KWANT package, for more details see, e.g., Refs. [S3, S4, S5].

1. Chebyshev polynomial expansion

The Chebyshev polynomials of the first kind are defined as

$$T_m(x) = \cos[m \arccos(x)] \quad (\text{C1})$$

on the interval $[-1, 1]$ and obey the orthogonality relation

$$\langle T_n, T_m \rangle_w = \frac{1 + \delta_{n,0}}{2} \delta_{n,m} \quad (\text{C2})$$

with respect to the scalar product defined by the weighting function $w(x) = [\pi\sqrt{1-x^2}]^{-1}$

$$\langle f, g \rangle_w = \int_{-1}^1 f(x)g(x)w(x)dx. \quad (\text{C3})$$

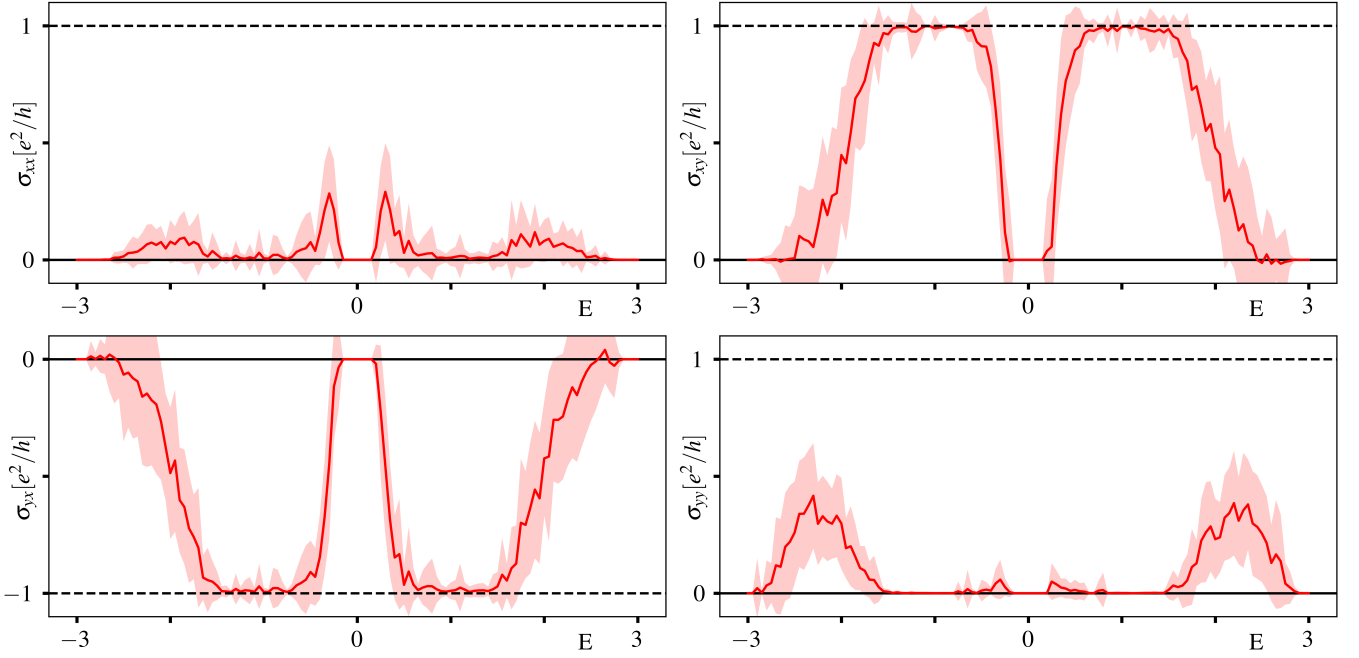


FIG. 6. Elements of the conductance tensor for a system size of $N_x = 2000$, $N_y = 500$ and parameters $r = 1.5$, $\epsilon_1 = 0.3$, $\epsilon_2 = 2$, $\gamma = 2$, $\gamma_2 = 0.3$ with disorder strength $W = 1.5$ as obtained from a standard four terminal scattering calculation. The leads attached to the vertical faces have a width of 50 unit cells and those at the horizontal faces have a width of 200 unit cells. The result is the average of $S = 40$ disorder realizations, standard deviation is indicated as a corridor.

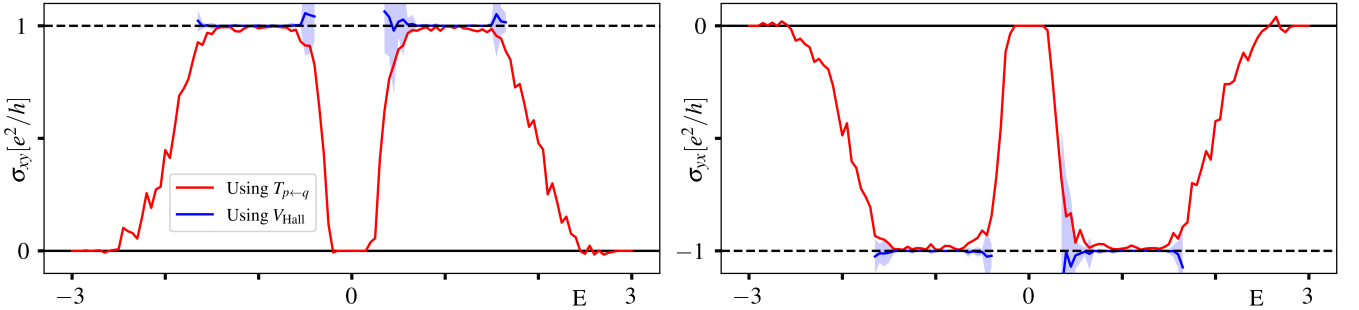


FIG. 7. Result for σ_{xy} and σ_{yx} for a system size of $N_x = 2000$, $N_y = 500$ and parameters $r = 1.5$, $\epsilon_1 = 0.3$, $\epsilon_2 = 2$, $\gamma = 2$, $\gamma_2 = 0.3$ with disorder strength $W = 1.5$. The leads attached to the vertical faces have a width of 50 unit cells and those at the horizontal faces have a width of 200 unit cells. We present the result obtained from extracting the Hall voltage from the conductance matrix in blue and compare it to the result obtained from the difference of the scattering amplitudes in red (same data as Fig. 6). The standard deviation of the blue curve is indicated as a corridor.

Another useful property is the recursion relation

$$T_{n+1}(x) = 2xT_n(x) - T_{n-1}(x). \quad (\text{C4})$$

For sufficiently regular functions on $[-1, 1]$, an expansion in T_n should converge uniformly and read

$$f(x) = 2 \sum_{n=0}^{\infty} \frac{\alpha_n T_n(x)}{\delta_{n,0} + 1} \quad (\text{C5})$$

with coefficients

$$\alpha_n = \langle f, T_n \rangle_w = \int_{-1}^1 f(x) T_n(x) w(x) dx. \quad (\text{C6})$$

To obtain an approximation to $f(x)$, this expansion can be truncated at some order M

$$f_M(x) = 2 \sum_{n=0}^{M-1} \frac{\alpha_n T_n(x)}{\delta_{n,0} + 1}, \quad (\text{C7})$$

however naively doing so will usually lead to so-called Gibbs oscillations. To obtain a better approximation, it is possible to fold the truncated function with a Kernel

$$f_{\text{KPM},M}(x) = \int_{-1}^1 \pi \sqrt{1-y^2} f_M(y) K_M(x,y) dy, \quad (\text{C8})$$

where the Kernel $K_M(x,y)$ depends on the order M of the approximation and can be chosen such that $f_{\text{KPM},M}(x)$ converges to $f(x)$ faster than the raw truncation $f_M(x)$. In practice, this amounts to multiplying the expansion coefficients by factors $g_n(M)$ that depend on the order M of the approximation:

$$f_{\text{KPM},M}(x) = 2 \sum_{n=0}^{M-1} g_n(M) \frac{\alpha_n T_n(x)}{\delta_{n,0} + 1}. \quad (\text{C9})$$

The optimal choice of Kernel depends on the nature of the problem at hand and which properties of the approximated functions should be preserved to obtain an accurate solution. The calculations in this paper employ the Jackson Kernel, which is well-suited for most physics applications and amounts to the choice

$$g_n = \frac{(M-n+1) \cos[\pi n/(M+1)] + \sin[\pi n/(M+1)] \cot[\pi/(M+1)]}{M+1}. \quad (\text{C10})$$

a. Extension to operator-valued functions

To apply the method to operator-valued functions of the Hamiltonian H , it has to be rescaled such that its spectrum is contained within $[-1, 1]$. This can be done by

$$H \rightarrow \tilde{H} = \frac{2}{\Delta_E} \left(H - \frac{E^+ + E^-}{2} \right), \quad E \rightarrow \tilde{E} = \frac{2}{\Delta_E} \left(E - \frac{E^+ + E^-}{2} \right), \quad (\text{C11})$$

where $\Delta_E = E^+ - E^-$ and E^\pm denote upper / lower bounds on the spectrum that can be estimated by Krylow methods. Then, any function $f(\tilde{E}, \tilde{H})$ of the rescaled Hamiltonian and an energy \tilde{E} can be expanded as

$$\begin{aligned} f(\tilde{E}, \tilde{H}) &= \sum_l f(\tilde{E}, \tilde{E}_l) |\tilde{E}_l\rangle \langle \tilde{E}_l| \\ &= \sum_l \left[2 \sum_{n=0}^{M-1} g_n(M) \alpha_n(\tilde{E}) T_n(\tilde{E}_l) \right] |\tilde{E}_l\rangle \langle \tilde{E}_l| \\ &= 2 \sum_{n=0}^{M-1} \frac{g_n(M) \alpha_n(\tilde{E})}{\delta_{n,0} + 1} T_n(\tilde{H}), \end{aligned} \quad (\text{C12})$$

where we applied the KPM expansion Eq. (C9) to the second argument of $f(\tilde{E}, \tilde{E}_l)$. Thus, the coefficients read (cf. Eq. (C6))

$$\alpha_n(\tilde{E}) = \int_{-1}^1 \frac{f(\tilde{E}, x) T_n(x)}{\pi \sqrt{1-x^2}} dx. \quad (\text{C13})$$

2. Expansion of the Kubo-Bastin formula

The exact linear response expression for the conductance tensor in a non-interacting system can be derived from the Kubo formula as

$$\sigma_{\alpha\beta}(E_F, T) = \frac{ie^2\hbar}{V} \int_{E^-}^{E^+} dE f_F(E - E_F, T) \text{Tr} \left[v_\alpha \frac{dG^+(E)}{dE} v_\beta \rho(E) - v_\alpha \rho(E) v_\beta \frac{dG^-(E)}{dE} \right], \quad (\text{C14})$$

where $f_{\text{F}}(E - E_{\text{F}}, T) = 1/(\exp[(E - E_{\text{F}})/(k_{\text{B}}T)] + 1)$ [S6, S7, S8]. Given the position operator R_{α} , the velocity operators follow from the Heisenberg picture as $v_{\alpha} = \dot{R}_{\alpha} = -(i/\hbar)[R_{\alpha}, H]$.

The other two relevant quantities are the DOS $\rho(E, H) = \delta(E - H)$ and the retarded/advanced GF $G^{\pm}(E, H) = [E \pm i0^{\pm} - H]^{-1}$. First of all, the above expression has to be rescaled in the sense of Eq. (C11). To this end, note that $\delta((\tilde{E} + b)/a - H) = |a|\delta(\tilde{E} - (aH - b)) = a\delta(\tilde{E} - \tilde{H})$ and $G^{\pm}[(\tilde{E} + b)/a, H] = [(\tilde{E} + b)/a - H + i0^{\pm}]^{-1} = a[\tilde{E} - \tilde{H} + ia0^{\pm}]^{-1} = aG^{\pm}[\tilde{E}, \tilde{H}]$, where $a = 2/\Delta_E$, $b = (E^+ + E^-)/\Delta_E$, from which we can infer by straightforward substitution

$$\sigma_{\alpha\beta}(E_{\text{F}}, T) = \frac{ia^2e^2\hbar}{V} \int_{-1}^1 d\tilde{E} f_{\text{F}}((\tilde{E} + b)/a - E_{\text{F}}, T) \text{Tr} \left[v_{\alpha} \frac{dG^+(\tilde{E})}{d\tilde{E}} v_{\beta} \rho(\tilde{E}) - v_{\alpha} \rho(\tilde{E}) v_{\beta} \frac{dG^-(\tilde{E})}{d\tilde{E}} \right]. \quad (\text{C15})$$

Now, the DOS and GF can be expanded as per Eq. (C12), with the coefficients following from Eq. (C13):

$$\alpha_{n,\rho}(\tilde{E}) = \int_{-1}^1 \frac{\delta(\tilde{E} - x) T_n(x)}{\pi\sqrt{1-x^2}} dx = \frac{T_n(\tilde{E})}{\pi\sqrt{1-\tilde{E}^2}} \quad (\text{C16})$$

$$\begin{aligned} \alpha_{n,G^{\pm}}(\tilde{E}) &= \int_{-1}^1 \frac{T_n(x)}{[\tilde{E} + i0^{\pm} - x]\pi\sqrt{1-x^2}} dx = \mathcal{P} \left[\int_{-1}^1 \frac{T_n(x)}{\pi[\tilde{E} - x]\sqrt{1-x^2}} dx \right] \mp i \frac{T_n(\tilde{E})}{\sqrt{1-\tilde{E}^2}} \\ &= U_{n-1}(\tilde{E}) \mp i \frac{T_n(\tilde{E})}{\sqrt{1-\tilde{E}^2}} = \mp i \frac{e^{\pm in \arccos(\tilde{E})}}{\sqrt{1-\tilde{E}^2}}. \end{aligned} \quad (\text{C17})$$

The real part of $\alpha_{n,G^{\pm}}(\tilde{E})$ is a standard integral relation between the Chebyshev polynomials of the first kind, $T_n(x)$, and the second kind $U_n(x) = \sin[(n+1)\arccos(x)]/\sqrt{1-x^2}$ [S5]. The derivative of $\alpha_{n,G^{\pm}}(\tilde{E})$ with respect to (w.r.t.) \tilde{E} is

$$\frac{d}{d\tilde{E}} \alpha_{n,G^{\pm}}(\tilde{E}) = \mp i \left[\frac{\tilde{E}}{(1-\tilde{E}^2)^{3/2}} \mp \frac{in}{1-\tilde{E}^2} \right] e^{\pm in \arccos(\tilde{E})}. \quad (\text{C18})$$

Having obtained the coefficients, we can expand Eq. (C15) as

$$\sigma_{\alpha\beta}(E_{\text{F}}, T) = \frac{4a^2e^2\hbar}{\pi V} \int_{-1}^1 d\tilde{E} \frac{f_{\text{F}}((\tilde{E} + b)/a - E_{\text{F}}, T)}{(1-\tilde{E}^2)^2} \sum_{m,n=0}^M \Gamma_{n,m}(\tilde{E}) \mu_{n,m}^{\alpha,\beta}, \quad (\text{C19})$$

where

$$\Gamma_{n,m}(\tilde{E}) = \left[\tilde{E} - in\sqrt{1-\tilde{E}^2} \right] e^{in \arccos(\tilde{E})} T_m(\tilde{E}) + T_n(\tilde{E}) \left[\tilde{E} + im\sqrt{1-\tilde{E}^2} \right] e^{-im \arccos(\tilde{E})} \quad (\text{C20})$$

does not depend on the details of the system, which are contained in

$$\mu_{n,m}^{\alpha,\beta} = \frac{g_n(M)g_m(M)}{(1+\delta_{n,0})(1+\delta_{m,0})} \text{Tr} [v_{\alpha} T_n(H) v_{\beta} T_m(H)]. \quad (\text{C21})$$

It is easily seen that $\Gamma_{m,n}^* = \Gamma_{n,m}$ and $(\mu_{m,n}^{\alpha,\beta})^* = \mu_{n,m}^{\alpha,\beta}$, which implies that Eq. (C19) is a real number. The numerical cost is hidden in the evaluation of $\mu_{m,n}^{\alpha,\beta}$, however the trace of a generic operator A can be sampled efficiently by using R random phase vectors $|\phi_l\rangle$:

$$\text{Tr}[A] \approx \frac{1}{R} \sum_{l=1}^R \langle \phi_l | A | \phi_l \rangle. \quad (\text{C22})$$

This estimate improves with system size N , it can be shown that for a generic operator A (in the sense of local and homogeneous support such that $\text{Tr}[A^2] = O(N^2)$) the relative error should scale as $\sim \frac{1}{\sqrt{NR}}$ [S5]. Furthermore, the recursion relation Eq. (C4) can be used to evaluate the scalar products appearing in the approximation of the trace.

To obtain the data presented in the main text of the paper, we used the efficient implementation of the algorithm outlined here in the KWANT package [S9, S10]. To generate correct velocity operators for PBC, we also acknowledge use of the extension KPM tools [S11].

Appendix D: Hall conductance of the clean system from the Kubo-Bastin formula

For completeness, we derive here that the Hall conductance of the clean system is indeed proportional to the accumulated Berry flux up to the Fermi energy E_F . At $T = 0$, the Hall conductance according to the Kubo-Bastin Formula can be written as

$$\sigma_{xy}(E_F, T = 0) = \frac{ie^2\hbar}{V} \int_{-\infty}^{E_F} dE \text{Tr} \left[v_x \frac{dG^+(E)}{dE} v_y \rho(E) - v_x \rho(E) v_y \frac{dG^-(E)}{dE} \right], \quad (\text{D1})$$

where all operators are to be interpreted as those arising from the single-particle tight-binding matrix [S6, S7, S8]. In the clean, translation-invariant system, all appearing quantities are block-diagonal in the momentum basis. The blocks of the velocity operators are readily derived to be $v_\alpha(\mathbf{k}) = \partial_{k_\alpha} H(\mathbf{k})/\hbar$, the GF terms become

$$\frac{dG^\pm(E, \mathbf{k})}{dE} = \frac{d}{dE} \sum_{l=1}^{N_O} \frac{1}{E + i0^\pm - E_l(\mathbf{k})} |E_l(\mathbf{k})\rangle \langle E_l(\mathbf{k})| = - \sum_{l=1}^{N_O} \frac{1}{(E + i0^\pm - E_l(\mathbf{k}))^2} |E_l(\mathbf{k})\rangle \langle E_l(\mathbf{k})|, \quad (\text{D2})$$

and the DOS

$$\rho(E, \mathbf{k}) = \sum_{l=1}^{N_O} \delta(E - E_l(\mathbf{k})) |E_l(\mathbf{k})\rangle \langle E_l(\mathbf{k})|. \quad (\text{D3})$$

The trace can be reduced to a sum over all \mathbf{k} and a trace over the eigenstates $|E_l(\mathbf{k})\rangle$ of the Bloch Hamiltonian at each \mathbf{k} (even though there might be topological obstructions to finding a smooth gauge for the $|E_l(\mathbf{k})\rangle$, this not a problem when taking the trace, as it is basis-independent). The Hall conductance thus becomes

$$\begin{aligned} \sigma_{xy}(E_F, T = 0) &= \frac{ie^2}{V\hbar} \int_{-\infty}^{E_F} dE \sum_{\mathbf{k}} \sum_{l, l'=1}^{N_O} \left[\langle E_l(\mathbf{k}) | (\partial_{k_x} H(\mathbf{k})) | E_{l'}(\mathbf{k}) \rangle \langle E_{l'}(\mathbf{k}) | (\partial_{k_y} H(\mathbf{k})) | E_l(\mathbf{k}) \rangle \frac{-\delta(E - E_l(\mathbf{k}))}{(E + i0^+ - E_{l'}(\mathbf{k}))^2} \right. \\ &\quad \left. - \langle E_l(\mathbf{k}) | (\partial_{k_x} H(\mathbf{k})) | E_{l'}(\mathbf{k}) \rangle \langle E_{l'}(\mathbf{k}) | (\partial_{k_y} H(\mathbf{k})) | E_l(\mathbf{k}) \rangle \frac{-\delta(E - E_{l'}(\mathbf{k}))}{(E + i0^- - E_l(\mathbf{k}))^2} \right]. \quad (\text{D4}) \end{aligned}$$

The terms of the above equation where $l = l'$ vanish, for the rest we can neglect the $i0^\pm$ regularization and carry out the integral to find

$$\begin{aligned} \sigma_{xy}(E_F, T = 0) &= - \frac{ie^2}{V\hbar} \sum_{\mathbf{k}} \sum_{l=1}^{N_O} \Theta(E_F - E_l(\mathbf{k})) \sum_{l' \neq l} \left[\langle E_l(\mathbf{k}) | (\partial_{k_x} H(\mathbf{k})) | E_{l'}(\mathbf{k}) \rangle \langle E_{l'}(\mathbf{k}) | (\partial_{k_y} H(\mathbf{k})) | E_l(\mathbf{k}) \rangle \right. \\ &\quad \left. - \langle E_l(\mathbf{k}) | (\partial_{k_y} H(\mathbf{k})) | E_{l'}(\mathbf{k}) \rangle \langle E_{l'}(\mathbf{k}) | (\partial_{k_x} H(\mathbf{k})) | E_l(\mathbf{k}) \rangle \right] \frac{1}{(E_l(\mathbf{k}) - E_{l'}(\mathbf{k}))^2} \\ &= - \frac{ie^2}{V\hbar} \sum_{\mathbf{k}} \sum_{l=1}^{N_O} \Theta(E_F - E_l(\mathbf{k})) \sum_{l' \neq l} \left[\langle \partial_{k_x} E_l(\mathbf{k}) | E_{l'}(\mathbf{k}) \rangle \langle E_{l'}(\mathbf{k}) | \partial_{k_y} E_l(\mathbf{k}) \rangle \right. \\ &\quad \left. - \langle \partial_{k_y} E_l(\mathbf{k}) | E_{l'}(\mathbf{k}) \rangle \langle E_{l'}(\mathbf{k}) | \partial_{k_x} E_l(\mathbf{k}) \rangle \right] \\ &= \frac{e^2}{V\hbar} \sum_{\mathbf{k}} \sum_{l=1}^{N_O} \Theta(E_F - E_l(\mathbf{k})) \left[-i \langle \partial_{k_x} E_l(\mathbf{k}) | \partial_{k_y} E_l(\mathbf{k}) \rangle - \langle \partial_{k_y} E_l(\mathbf{k}) | \partial_{k_x} E_l(\mathbf{k}) \rangle \right] \\ &= \frac{e^2}{\hbar} \sum_{l=1}^{N_O} \frac{1}{2\pi} \int d^2k \Theta(E_F - E_l(\mathbf{k})) \mathcal{F}_l(\mathbf{k}) = \frac{e^2}{\hbar} \sum_{l=1}^{N_O} \frac{1}{2\pi} \int_{E_l(\mathbf{k}) < E_F} d^2k \mathcal{F}_l(\mathbf{k}). \quad (\text{D5}) \end{aligned}$$

For the second equality above, we used that $\langle E_l(\mathbf{k}) | (\partial_{k_\alpha} H(\mathbf{k})) | E_{l'}(\mathbf{k}) \rangle = \langle \partial_{k_\alpha} E_l(\mathbf{k}) | E_{l'}(\mathbf{k}) \rangle [E_l(\mathbf{k}) - E_{l'}(\mathbf{k})] = - \langle E_l(\mathbf{k}) | \partial_{k_\alpha} E_{l'}(\mathbf{k}) \rangle [E_l(\mathbf{k}) - E_{l'}(\mathbf{k})]$ and for the third equation, we note that the term $l' = l$ yields zero and can formally be added to the sum $\sum_{l' \neq l}$ to yield a resolution of identity. Finally, the continuum limit is taken as $\Delta_{\mathbf{k}}^2 \sum_{\mathbf{k}} = \int d^2k$ with $\Delta_{\mathbf{k}}^2 = 4\pi^2/V$.

Appendix E: Additional data on the spectral localizer

We calculate the localizer gap for different system sizes and find that it saturates at $N_x = N_y = N = 15$. The data is presented in Fig. 8. We note that the sign of the topological index Q obtained from the spectral localizer is opposite to that of the observed Hall conductance in the presence of disorder, which is due to a different sign convention for the Berry curvature. The spectral localizer framework takes the Berry curvature as $F_n = i(\nabla \times \langle n | \nabla | n \rangle) \cdot \mathbf{e}_z$ (see Eq. (1) of Ref. [S13]) as opposed to the usual convention $F_n = -i(\nabla \times \langle n | \nabla | n \rangle) \cdot \mathbf{e}_z$ (see chapter three of Ref. [S12]) used in the physics context. The latter should produce an equal sign of Chern number and Hall conductance as we also derive in Eq. (D5).

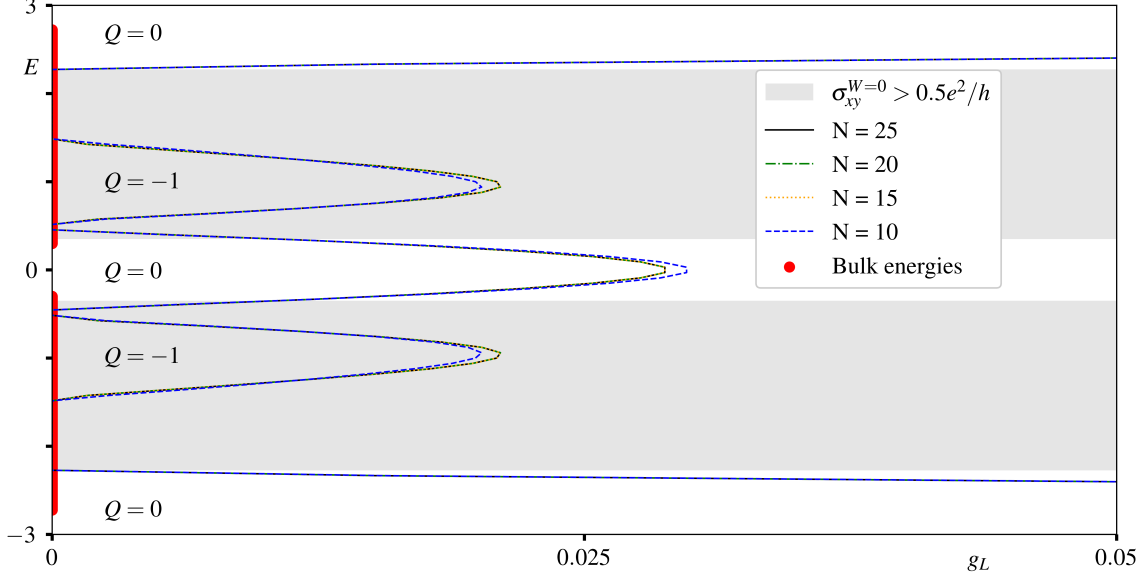


FIG. 8. Localizer gap g_L [cf. Eq. (6)] as a function of energy for parameters $r = 1.5$, $\epsilon_1 = 0.3$, $\epsilon_2 = 2$, $\gamma = 2$, and $\gamma_2 = 0.3$ for multiple system sizes of $N_x = N_y = N$. The scaling parameter is set to $\kappa = 0.4$. The value of g_L is taken as the minimum of 100 reference positions inside the central Wigner-Seitz cell. Wherever the localizer gap is stable, we indicate the associated value of the topological index Q [cf. Eq. (7)]. For reference, the clean bulk spectrum is shown in red and the energy window where $\sigma_{xy}^{W=0}(E_F) > 0.5e^2/h$ [cf. Eq. (2)] is marked as a gray corridor.

We note that there is an extended energy window in Fig. 8 where the localizer gap is zero. In principle, this is expected as the existence of a finite localizer gap is only guaranteed in the presence of a spectral gap [S13] or a mobility gap under [S14]. For energies in the bulk of the clean system, there is neither a spectral nor a mobility gap and thus no guarantee for a conclusive statement on the topology of the system from the spectral localizer. However, our numerical data strongly indicates a stable localizer gap for certain energy windows in the bulk of the clean system. Assuming that this gap is indeed stable in the thermodynamic limit, the usual argument for the topological stability of the localizer gap and associated topological indices based on Weyl's inequality [S13, S15] can be extended to the present situation. If we order the eigenvalues of two Hermitian operators A and B defined on an n -dimensional vector space as $\lambda_1 \geq \lambda_2 \geq \dots \geq \lambda_n$, Weyl's inequality states that $\lambda_i(A) + \lambda_j(B) \leq \lambda_{i+j-n}(A+B)$. By setting $j = 1$ and $i = n$, it follows that $\lambda_1(A+B) - \lambda_1(B) \in [\lambda_n(B), \lambda_1(B)]$ and thus

$$|\lambda_i(A+B) - \lambda_i(A)| \leq \|B\|_2, \quad (\text{E1})$$

where $\|B\|_2 = \max\{|\lambda_1(B)|, |\lambda_n(B)|\}$ denotes the L_2 matrix norm, i.e. the maximum modulus of the eigenvalues. Setting $A = L^{\hat{H}_0}(x, y, E)$ and $B = L^{\hat{H}_0 + \hat{W}}(x, y, E) - L^{\hat{H}_0}(x, y, E) = \sigma_z \otimes \hat{W}$, where we denote by $L^{\hat{H}}(x, y, E)$ the spectral localizer for a Hamiltonian \hat{H} , leads to

$$\left| \lambda_i \left[L^{\hat{H}_0 + \hat{W}}(x, y, E) \right] - \lambda_i \left[L^{\hat{H}_0}(x, y, E) \right] \right| \leq \|L^{\hat{H}_0 + \hat{W}}(x, y, E) - L^{\hat{H}_0}(x, y, E)\|_2 = \|\hat{W}\|_2. \quad (\text{E2})$$

This means that the change of any eigenvalue of $L^{\hat{H}_0 + \hat{W}}(x, y, E)$ relative to that of $L^{\hat{H}_0}(x, y, E)$ is bounded by the maximum eigenvalue of \hat{W} . It follows for finite $g_{L^{\hat{H}_0}}(E)$ that as long as $\|\hat{W}\|_2 < g_{L^{\hat{H}_0}}(E)$, the localizer gap in the bulk

at energy E cannot close in the presence of the disorder potential. However, a finite value of the disorder strength should still lead to Anderson localization and the formation of a mobility gap in the thermodynamic limit, which would make the topological localizer index Q well-defined. It should thus agree with the expected value of the Hall conductance in the presence of disorder already in the clean system, which is what we observe.

To conclude this section, we would like to emphasize that we do not make any analytical argument for a finite localizer gap in the absence of a spectral or mobility gap, but only observe it as a numerical fact. It remains an interesting direction for future research whether mathematically rigorous statements can be made in this regard.

Appendix F: Relation to "Topological fine structure of an energy band"

In a recent work [S15], it has been observed that a trivial band that is coupled to two bands with Chern numbers ± 1 can split in two non-trivial bands in the presence of disorder. This is also accompanied by a finite and non-trivial localizer gap inside the bulk energies of the clean system. However, a deeper physical reason for this remains elusive. We find that our present approach of relating the topological structure emerging from a trivial band in the presence of disorder to an energetic separation of Berry fluxes agrees well with the numerical observations made in Ref. [S15].

Concretely, the model under investigation in Ref. [S15] is given by

$$H(\mathbf{k}) = \begin{pmatrix} h_{11}(\mathbf{k}) & h_{12}(\mathbf{k}) & v \\ h_{12}(\mathbf{k})^* & -h_{11}(\mathbf{k}) & 0 \\ v & 0 & 0 \end{pmatrix} \quad (\text{F1})$$

with $h_{11}(\mathbf{k}) = 2(\cos(k_x) - \cos(k_y))$ and $h_{12}(\mathbf{k}) = \sqrt{2}e^{-i\pi/4}(e^{ik_x} + e^{ik_y} + i(e^{i(k_x+k_y)} + 1))$. The top left 2×2 block describes two topological bands with Chern number $C = \pm 1$ and the term v couples them to a third band centered at $E = 0$ that is trivial and completely flat for $v = 0$. A phase transition occurs at $v \approx 5.65$, where the $C = \pm 1$ bands simultaneously touch the middle band and revert to trivial bands. At small coupling v , transport calculations in the presence of disorder (also performed using KWANT) show that the middle band localizes while the top and bottom bands flow together and annihilate, which is the expected behavior. However, for $3.3 \lesssim v \lesssim 5.65$, the trivial middle band starts to split into two subbands that annihilate with the already present topological bands. Please see Ref. [S15] for data and details.

To obtain the clean Hall conductance in the sense of Eq. (D5) of the Hamiltonian Eq. (F1), an efficient algorithm for calculating the Berry curvature such as Ref. [S16] can be used. We present the result for different values of the coupling v in Fig. 9 and find that it predicts the behavior of the system under disorder observed in Ref. [S15] rather well. For $v = 2$, there is no energy in the central band where $\sigma_{xy} < 0.5e^2/h$, as Fig. 9(a) shows. Consequently, one would expect that disorder simply straightens out the line and leads to one big Hall plateau, which is equivalent to completely localizing the middle band. Moving to $v = 3.3$ in Fig. 9(b), an energy window opens where $\sigma_{xy} < 0.5e^2/h$, in which a trivial phase with $\sigma_{xy} = 0$ should form at the onset of disorder. At $v = 4.5$ in Fig. 9(c), the window $\sigma_{xy} < 0.5e^2/h$ broadens, suggesting a similar behavior to the case of $v = 3.3$. Finally, Fig. 9(d) shows the case of $v = 6.5$, which is past the quantum phase transition. There, $\sigma_{xy} < 0.5e^2/h$ everywhere, which is consistent with a complete localization of all bands in the presence of disorder. In summary, the expectations from the evaluation of the clean Hall conductance in Fig. 9 fully agree with the numerical results of Ref. [S15], which suggests that Eq. (D5) is a versatile tool to gain physical insight into the topological fine structure of energy bands.

- [S1] S. Datta, *Electronic Transport in Mesoscopic Systems*, Cambridge (1995).
- [S2] G. Salerno, H. M. Price, M. Lebrat, S. Häusler, T. Esslinger, L. Corman, J.-P. Brantut, and N. Goldman, *Quantized Hall Conductance of a Single Atomic Wire: A Proposal Based on Synthetic Dimensions*, *Phys. Rev. X* **9**, 041001 (2019).
- [S3] J. H. Garcia, L. Covaci, T. G. Rappoport, *Real-space calculation of the conductivity tensor for disordered topological matter*, *Phys. Rev. Lett.* **114**, 116602 (2015).
- [S4] D. Ködderitzsch, K. Chadova, and H. Ebert, *Linear response Kubo-Bastin formalism with application to the anomalous and spin Hall effects: A first-principles approach*, *Phys. Rev. B* **92**, 184415 (2015).
- [S5] A. Weisse, G. Wellein, A. Alvermann, H. Fehske, *The Kernel Polynomial Method*, *Rev. Mod. Phys.* **78**, 275 (2006).
- [S6] R. Kubo, *Statistical-Mechanical Theory of Irreversible Processes. I. General Theory and Simple Applications to Magnetic and Conduction Problems*, *Journal of the Physical Society of Japan* **12**, pp. 570-586 (1957).
- [S7] A. Bastin, C. Lewinler, O. Betbeder-Matibet, and P. Nozieres, *Quantum oscillations of the hall effect of a fermion gas with random impurity scattering*, *J. Phys.*

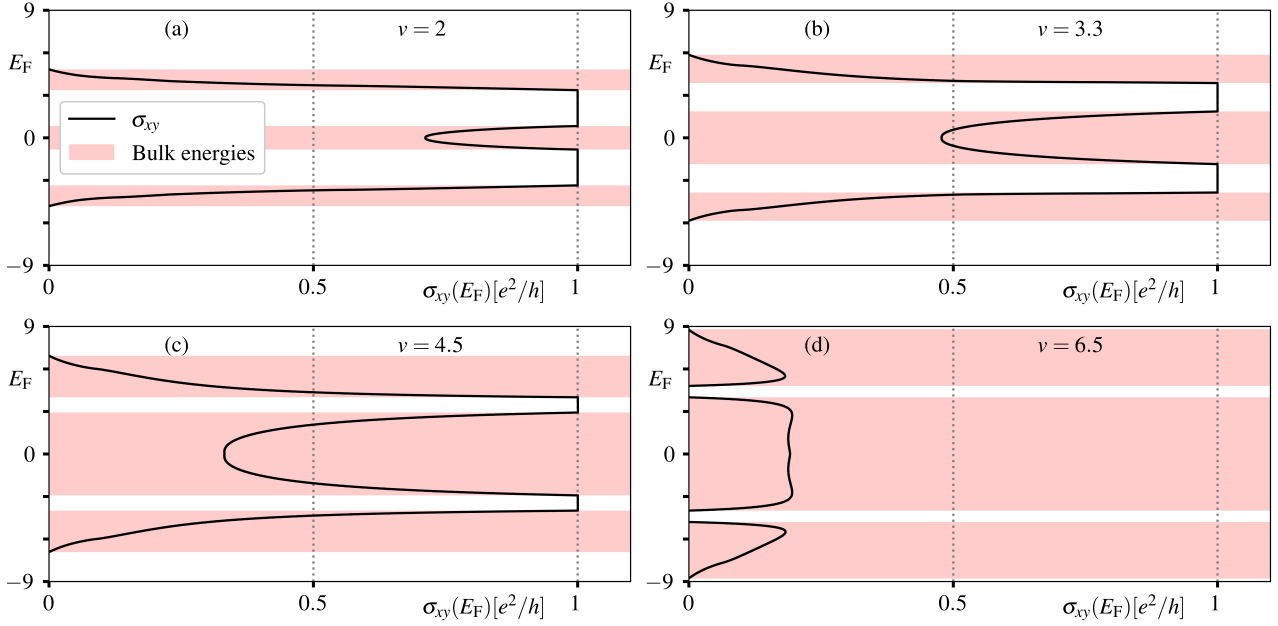


FIG. 9. Clean Hall conductance σ_{xy} of the Hamiltonian Eq. (F1) as a function of Fermi energy E_F for different coupling strengths v . The energy windows of the bulk bands are indicated as corridors for reference. The following description of subfigures states the value of v and the behavior observed in Ref. [S15] for the respective value. (a) $v = 2$, σ_{xy} does not dip below $0.5e^2/h$, in the central band. The central band does not split in the presence of disorder, but simply localizes. (b) $v = 3.3$, an energy window emerges where $\sigma_{xy} < 0.5e^2/h$. The central band begins to split and annihilate with the upper and lower band in the presence of disorder. (c) $v = 4.5$, the window where $\sigma_{xy} < 0.5e^2/h$ broadens and the response to disorder is similar to $v = 3.3$. (d) $v = 6.5$, the bands have touched and a phase transition has occurred such that $\sigma_{xy} < 0.5e^2/h$ everywhere. All bands are trivial and simply localize at the onset of disorder.

Chem. Solids **32**, 1811 (1971).

- [S8] A. Crépieux and P. Bruno, *Theory of the anomalous Hall effect from the Kubo formula and the Dirac equation*, *Phys. Rev. B* **64**, 014416 (2001).
- [S9] C. W. Groth, M. Wimmer, A. R. Akhmerov, X. Waintal, *Kwant: a software package for quantum transport*, *New J. Phys.* **16**, 063065 (2014).
- [S10] P. R. Amestoy, I. S. Duff, J. S. Koster, J. Y. L'Excellent, *Accelerating Optimization of Parametric Linear Systems by Model Order Reduction*, *SIAM. J. Matrix Anal. & Appl.* **23** (1), 15 (2014).
- [S11] To implement the Kubo-Bastin formula with PBC, we use the KWANT extension **KPM Tools**, which is largely based on ideas from: D. Varjas, M. Fruchart, A. R. Akhmerov, P. M. Perez-Piskunow, *Computation of topological phase diagram of disordered $\text{Pb}_{1-x}\text{Sn}_x\text{Te}$ using the kernel polynomial method*, *Phys. Rev. Research* **2**, 013229 (2020).
- [S12] B. A. Bernevig, T. L. Hughes *Topological insulators and topological superconductors*, *Princeton University Press*, 2013.
- [S13] A. Cerjan and T. A. Loring, *Tutorial: Classifying Photonic Topology Using the Spectral Localizer and Numerical K -Theory*, *APL Photonics* **9**, 111102 (2024)
- [S14] T. Stoiber, *A spectral localizer approach to strong topological invariants in the mobility gap regime*, *arXiv:2410.22214* (2024).
- [S15] H. Liu, C. Fulga, E. J. Bergholtz, J. K. Asboth, *Topological fine structure of an energy band*, *arXiv:2312.08436* (2023).
- [S16] T. Fukui, Y. Hatsugai, and H. Suzuki, *Chern Numbers in Discretized Brillouin Zone: Efficient Method of Computing (Spin) Hall Conductances*, *J. Phys. Soc. Jpn.* **74**, pp. 1674-1677 (2005)